High-spin structure and electromagnetic transition strengths in Cd-104

Muller, G. A.; Jungclaus, A.; Yordanov, O.; Galindo, E.; Hausmann, M.; Kast, D.; Lieb, K. P.; Brant, Slobodan; Krstić, Vladimir; Vretenar, Dario; ...

High-spin structure and electromagnetic transition strengths in ^{104}Cd

G. A. Müller, A. Jungclaus, O. Yordanov, E. Galindo, M. Hausmann, D. Kast, and K. P. Lieb
II. Physikalisches Institut, Universität Göttingen, Bunsenstrasse 7-9, D-37073 Göttingen, Germany

S. Brant, V. Krstić, and D. Vretenar
Department of Physics, Faculty of Science, University of Zagreb, 10000 Zagreb, Croatia

A. Algora, F. Brandolini, G. de Angelis, M. De Poli, C. Fahlander, A. Gadea, T. Martinez, and D. R. Napoli
Istituto Nazionale di Fisica Nucleare, Laboratori Nazionali di Legnaro, I-35020 Legnaro, Italy

A. Dewald, R. Peusquens, and H. Tiesler
Universität zu Köln, Zülpicher Strasse 77, D-50937 Köln, Germany

M. Górska and H. Grawe
Gesellschaft für Schwerionenforschung, D-64291 Darmstadt, Germany

P. G. Bizzeti
Istituto Nazionale di Fisica Nucleare, Sezione di Firenze, I-50125 Firenze, Italy
(Received 26 January 2001; published 4 June 2001)

The recoil-distance Doppler-shift and Doppler-shift attenuation techniques were employed to determine for the first time lifetimes of high-spin states in ^{104}Cd in the time range 0.3 ps$\leqslant\tau\leqslant$1.2 ns. The nuclei were populated using the compound nucleus reaction ^{58}Ni(^{50}Cr, $4p$) and the γ radiation from their decay was detected with the GASP spectrometer. A total of 34 reduced transition probabilities and limits for 18 further transitions were extracted providing a rich basis for a comparison with theoretical calculations. In addition, the lifetime data contained new information urging for a revision of the published level scheme of ^{104}Cd. In particular, a magnetic dipole band recently established and interpreted as magnetic rotation is shown to be not existing. The new experimental results in ^{104}Cd are discussed in the frame of the interacting boson plus broken pair model.

DOI: 10.1103/PhysRevC.64.014305 PACS number(s): 21.10.Tg, 21.10.Ky, 21.60.Fw, 27.60.+j

I. INTRODUCTION

The light Cd isotopes with two proton holes and only a couple of neutrons outside the ^{100}Sn core exhibit at low spin the typical behavior of vibrating nearly spherical nuclei. Using the angular projected generator coordinate method and the finite range density dependent Gogny force [1], the ground state of the nucleus ^{104}Cd was found to be a superposition of prolate ($\beta\approx0.15$) and oblate ($\beta\approx-0.12$) configurations [2]. The softness of this nucleus with respect to collective vibrations and the competition between single particle levels of different structure clearly illustrate the difficulty to interpret the experimental information in terms of simple configurations as well as to perform *ab initio* calculations that should include many degrees of freedom. In the heavier Cd isotopes with $A=106-110$ weakly deformed rotational structures based on the $(\nu h_{11/2})^2_{10^+}$ neutron intruder configuration have been observed. In a recent publication by de Angelis *et al.* [3], the high-spin part of the level scheme of ^{104}Cd known from previous work [4] has been considerably extended. States of both parities have been observed up to excitation energies of ≈10 MeV. In this work, the interacting boson plus broken pair model (IBBPM), which allows a simultaneous treatment of the vibrational, the rotational, and the noncollective single-particle degrees of freedom, has been used to describe the excitation scheme of ^{104}Cd. Different two-neutron configurations based on the $d_{5/2}$, $g_{7/2}$, and $h_{11/2}$ orbits have been assigned to the experimentally observed structures. Jenkins *et al.* [5] very recently observed a magnetic dipole band that they interpreted as magnetic rotation.

So far, except for the decay of the 8^+ isomer at 2904 keV [$\tau=1.23(7)$ ns [6]], no experimental information about the electromagnetic decay properties of the high-spin states in ^{104}Cd was available. Whereas magnetic moment measurements have shown that the yrast 8^+ states in the lighter neighbors ^{100,102}Cd are of rather pure $(\pi g_{9/2})^2$ nature, both the decreasing lifetime of the 8^+ state with increasing neutron number as well as the observation of four 8^+ levels within 400 keV and three 6^+ states within 160 keV in ^{104}Cd [3] indicate a larger configuration mixing in this nucleus (note, however, that one 6^+ and one 8^+ state established in Ref. [3] will be shown in the present work to be not existent). To pin down the two-neutron, two-proton, or collective character of these states, information on electromagnetic transition rates is crucial. We therefore performed a detailed investigation of the lifetimes of high-spin states in ^{104}Cd employing both the recoil-distance Doppler-shift (RDDS) and the Doppler-shift attenuation (DSA) techniques. A second motivation for this study was to use the lifetime information in order to clarify the discrepancies between the level schemes of ^{104}Cd published in Refs. [3–5]. To interpret the

new experimental information, extended IBBPM calculations including configurations with both broken proton and neutron pairs were performed. The advantage of this calculation compared to the one presented in Ref. [3] is that now high-spin bands based on two-proton and two-neutron configurations can simultaneously be described.

The paper is composed in the following way. In Sec. II, some details about the two experiments performed to study ^{104}Cd are presented. The revision of the published level scheme that became necessary in view of the new information is illustrated in Sec. III. In the main part of this paper, the determination of picosecond lifetimes using the differential decay curve method (DDCM), RDDS and DSA methods is described in detail (Sec. IV) followed by a discussion of the results in comparison to calculations within the interacting boson with broken pair model in Sec. V. The paper closes with the conclusions.

II. EXPERIMENTS

In both experiments, the ^{104}Cd nuclei have been populated using the compound nucleus reaction ^{58}Ni(^{50}Cr, $4p$) and the γ rays from the decay of the highly excited nuclei have been detected in the GASP spectrometer (configuration II in the plunger and configuration I in the DSA experiment) consisting of 40 Compton-suppressed HPGe detectors [7]. The ^{50}Cr beam with energies of 205 MeV in the plunger and 200 MeV in the DSA experiment, respectively, has been delivered by the Tandem XTU accelerator of the Legnaro National Laboratories. In the plunger experiment, the target consisted of a stretched 1.2-mg/cm^2-thick ^{58}Ni foil (enriched to 99.8%) mounted in the Cologne plunger device [8]. The nuclei have been stopped in a 12.3-mg/cm^2-thick gold foil at 12 different distances between 16 μm and 7 mm from the target. The recoil velocity of the ^{104}Cd nuclei was deduced from the energy shift between stopped and Doppler-shifted components of intense γ transitions to be $v = 9.61(19)$ μm/ps or 3.20(6)% of the speed of light. Further details about this experiment are given in [9]. In the second experiment, performed to measure short lifetimes using the DSA technique, a target consisting of a 1.0-mg/cm^2-thick ^{58}Ni layer (enrichment 99.8%) on a 15-mg/cm^2-thick gold foil has been used. At the chosen beam energies, the $4p$ channel ^{104}Cd is one of the strongest reaction channels observed [10].

In both experiments, triple- or higher-fold coincidence events with a maximum of two γ rays in the 90° detector ring of the GASP spectrometer were registered on tape. Energy and efficiency calibrations of the spectra and gain matching of the individual Ge detectors were performed offline using standard γ ray sources (^{133}Ba, ^{152}Eu, and ^{56}Co) for energies from 70 keV to 3.9 MeV.

To prepare the data for the lifetime analysis, for each of the 12 flight distances in the plunger experiment as well as for the DSA measurement, the events on tape were unfolded and sorted into asymmetric matrices. Since the 40 Ge detectors of the GASP array can be grouped into seven rings of roughly the same angle Θ relative to the beam ($\Theta = 35°$, 59°, 72°, 90°, 108°, 121°, and 145°), 28 different matrices with one particular ring on each axis were sorted with gates to be set in all seven rings and spectra accumulated only in the rings at 35°, 59°, 121°, and 145°. No spectra were analyzed in the 72°, 90°, and 108° rings where the Doppler shift is smallest and therefore the separation between shifted and unshifted components of the γ lines poorest.

From the data of the DSA experiment, two additional matrices were sorted. The first one is a symmetric matrix containing all unfolded $\gamma\gamma$ events. Since this matrix served for checking the published level scheme, it was constructed with a high energy dispersion of only 0.5 keV per channel allowing a detailed analysis of multiplet structures. A matrix with the γ rays detected in the 90° ring on one axis and γ rays observed at 35° or 145° on the other axis allowed the determination of γ ray multipolarities from the analysis of the directional correlation ratios from oriented states (DCO) for transitions in ^{104}Cd. Using a coincidence gate on a stretched quadrupole transition γ_{gate}, the DCO ratio

$$R_{DCO} = \frac{I_\gamma(\gamma \text{ observed at } \Theta_1; \gamma_{gate} \text{ at } \Theta_2)}{I_\gamma(\gamma \text{ observed at } \Theta_2; \gamma_{gate} \text{ at } \Theta_1)} \frac{\epsilon_{\Theta_1}(\gamma)\epsilon_{\Theta_2}(\gamma_{gate})}{\epsilon_{\Theta_1}(\gamma_{gate})\epsilon_{\Theta_2}(\gamma)} \tag{1}$$

is ≈ 1 for stretched quadrupole and ≈ 0.5 for pure dipole transitions. On the contrary, using a gate on a pure dipole transition, the expected DCO ratios for quadrupole and dipole transitions are ≈ 2 and ≈ 1, respectively. $\epsilon_\Theta(\gamma)$ is the relative efficiency at the energy E_γ of the detectors positioned at angle Θ with respect to the beam.

III. REVISION OF THE LEVEL SCHEME OF ^{104}Cd

The most comprehensive level scheme of the nucleus ^{104}Cd so far has been presented in the work of de Angelis *et al.* [3]. There, the same reaction as in the present work, however at a higher beam energy of 220 MeV, self-supporting ^{58}Ni foils as targets, the GASP array for γ ray and in addition the Si-ball ISIS for charged particle detection have been used. In a very recent publication, Jenkins *et al.* [5] presented a revised version of the level scheme, based on thick and thin target experiments using the reaction ^{54}Fe(^{58}Ni, $\alpha 4p$) at 243 MeV and the Gammasphere spectrometer in combination with the microball charged particle detector system. The main difference between the two versions of the level scheme is the structure of the levels above

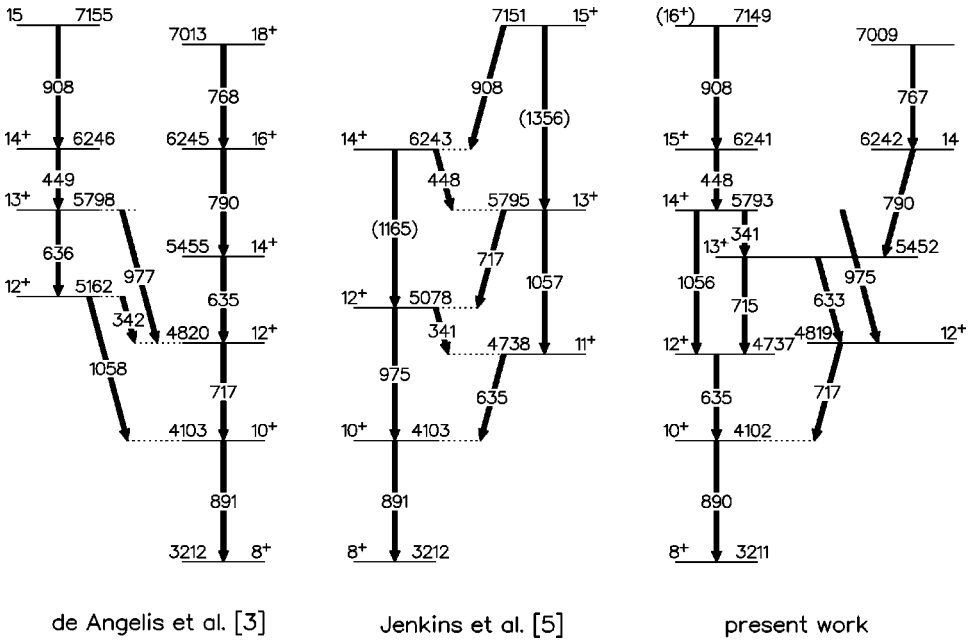

FIG. 1. Relevant parts of the level schemes of ^{104}Cd established in [3,5]. In comparison, the revised version obtained in the present work is presented on the right-hand side.

the 10^+ state at 4103 keV, where Jenkins *et al.* [5] reordered the transitions in such a way to form a magnetic dipole band. To facilitate the following discussion, the relevant parts of the level schemes from the two publications are shown in Fig. 1. We used two different sources of information to check which of the two versions, if any, is correct. First, the decay curves of individual γ transitions obtained in the plunger experiment contain information about the ordering of the transitions. Contradictions arise, for example, from the observation of very different decay curves for two γ rays depopulating the same state. In addition, we carefully searched for multiplet structures with the help of the coincidence matrix constructed with an energy resolution of 0.5 keV per channel.

Figure 2(a) shows the decay curve of the 717-keV transition obtained in the coincidence spectrum with gate on the 890-keV $10^+ \rightarrow 8^+$ transition. $R(x)$ denotes as usual the intensity of the unshifted component of the transition observed at the flight distance x normalized to the number of reactions observed at the different distances. It is obvious at first sight that this curve cannot be described by a single exponential decay but rather contains two components, a short one and a longer one, leading to a shoulder at around 50 μm. Such a shape results if the decaying state is populated by two discrete feeders with different decay constants. In the level scheme proposed by de Angelis *et al.* [3], the 12^+ level depopulated by the 717-keV transition has three main feeding transitions, namely the γ rays with 342, 977, and 635 keV. The 342 and 977 keV transitions have short decay constants as shown in Fig. 3. That means that to explain the shape of the 717-keV decay curve, the 635-keV $14^+ \rightarrow 12^+$ feeder must have a long time constant. Since the 635-keV transition is a doublet, we compare the decay curves of the 342-keV and 635-keV transitions deduced in coincidence with the 717-keV γ ray. The difference of these two curves shown in Fig. 2(b) corresponds to the intensity of the $14^+ \rightarrow 12^+$ component of the doublet. Obviously, this third feeder of the 12^+ state has a short time constant, too. To conclude, assuming the level structure shown on the left in Fig. 1, the decay curve of the 717-keV transition cannot be explained.

Evaluating the same information now with respect to the level sequence proposed by Jenkins *et al.* [5], we find two

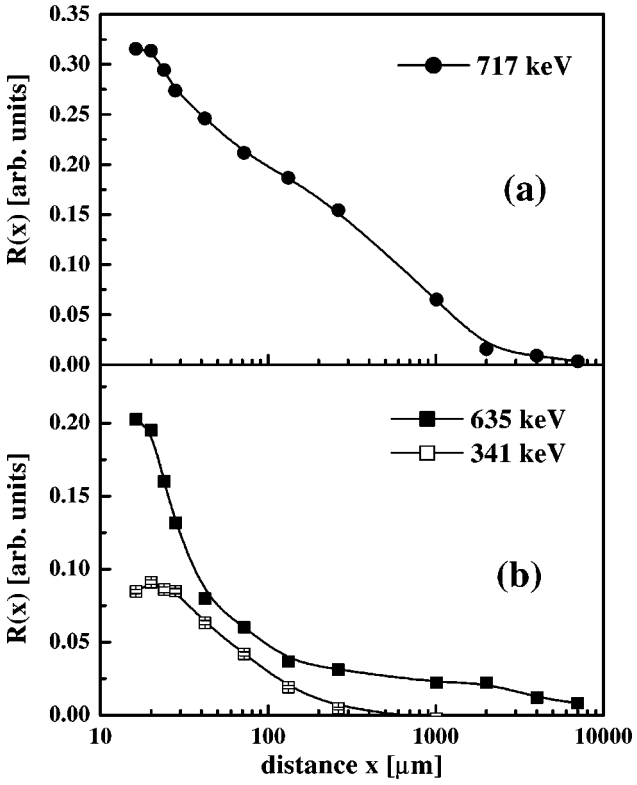

FIG. 2. (a) Decay curve of the 717-keV transition deduced in the coincidence spectrum with gate on the 890-keV $10^+ \rightarrow 8^+$ transition, (b) decay curves of the 341-keV and 635-keV transitions deduced in the coincidence spectrum with gate on the 717-keV transition.

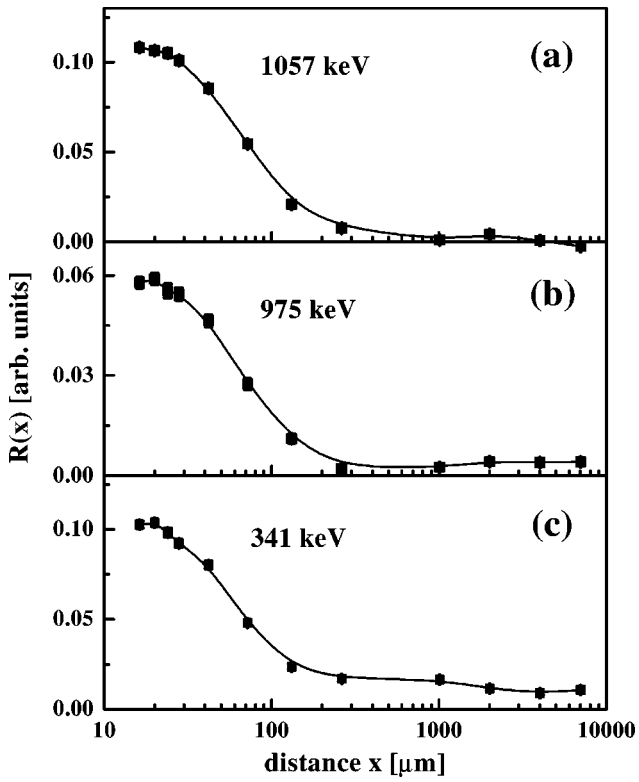

FIG. 3. Decay curves of the 341-keV, 975-keV, and 1056-keV transition deduced in the coincidence spectrum with gate on the 890-keV transition.

severe contradictions. First, according to this scheme, the two transitions depopulating the 13^+ state, namely the γ rays with 717 keV and 1057 keV, must reflect the same decay history which is certainly not the case [compare Fig. 2(a) and 3(a)]. Secondly, neither the 341-keV nor the 975-keV decay curves (see Fig. 3) show any long component as expected assuming the 717-keV transition to be the prominent feeder. The bad intensity balance for the 12^+ state as deduced from the intensities quoted in Table I of Ref. [5] [I_{in}(717 keV) $=18.2(3)$, I_{out}(341 keV+975 keV)$=11.9(3)$] might further reduce the confidence in the proposed level scheme.

The key for establishing the correct level sequence has been a careful analysis of the 717-keV line. This line as observed under different gating conditions is shown in Fig. 4. The coincidence gate on the 890-keV transition reveals the doublet structure of the 717-keV line. By gating on individual channels of this line, we found that the center of the coincident 635-keV line is shifting too, leading to the result that there is a 635-keV transition in coincidence with a 715-keV line and a 633-keV γ ray in coincidence with one at 717 keV. In the next step, the position of the transitions in the level scheme has been fixed with the help of the coincidence spectra with gates set on the 341-keV, 975-keV, and 1056-keV lines, partly shown in Figs. 4 and 5. The analysis of these spectra implies without contradiction the level ordering shown on the right in Fig. 1. It is further supported by the measured DCO ratios of the transitions involved. For the 717- and 635-keV transitions, DCO ratios of 0.90(6) and 0.92(5) were obtained gating on the $E2$ transitions 975 and 1056 keV, respectively, the quadrupole character of which was determined in gates on the ground state transition. The values obtained in our DCO analysis are in clear contradiction to the $M1$ assignments for the 635- and 717-keV transitions made by Jenkins *et al.* [5]. The analysis of the doublets in the gate on the 890-keV transition indicates that the weaker components of both doublets, namely the γ rays with 633 and 715 keV, are of dipole nature [R_{DCO}(633 keV) $=0.56(5)$, R_{DCO}(635 keV)$=0.93(5)$, R_{DCO}(715 keV) $=0.44(3)$, and R_{DCO}(717 keV)$=1.11(7)$ in the 890-keV gate] leading unambiguously to the spin assignments shown in Fig. 1. Since we observed a weak self-coincidence of the 635-keV line, a second transition with this energy has been placed higher up in the cascade as $(18^+)\rightarrow(17^+)$ transition. However, the level order within this cascade above the 15^+ state at 6241 keV is only based on the intensities of the transitions and has to be regarded as tentative.

There is a second region in the level scheme in which, based on the present lifetime information, we would like to suggest a revision of the level ordering proposed in Ref. [3]. In Ref. [3], the 10^+ yrast state at 3656 keV is connected to the 4^+ level at 1493 keV via the γ ray sequence 623 keV, 500 keV, and 1040 keV ($10^+_1\rightarrow8^+_2\rightarrow6^+_3\rightarrow4^+_1$). Since no additional populating or depopulating transitions of the 8^+_2 and the 6^+_3 levels were observed, the ordering has been chosen based on the γ ray intensities. However, using the argument that in the coincidence spectrum with the gate on the unshifted component of a feeding transition only the unshifted part of a depopulating transition can be observed, we suggest the correct order to be 1040-622-500 keV. The relevant parts of the coincidence spectra with gates on the 500-keV and 622-keV transitions taken at four different angles and two different flight distances are shown in Fig. 6. Since Doppler-shifted components of both the 622-keV and the 1040-keV transitions are observed in coincidence with the unshifted part of the 500-keV line [compare Figs. 6(a),(b)], the 500-keV γ ray has to be lowest in the sequence. Similarly, the 1040-keV γ ray has to be placed above the 622-keV transition since it is observed in flight in the gate on the unshifted component of the 622-keV line [see Fig. 6(c)]. Concerning the spins of the 1992-keV, 2614-keV, and 3654-keV states, the situation is difficult. Following de Angelis *et al.* [3], where all three transitions have been assigned $E2$ character, the 1992-keV level is the new 6^+ yrast and the 2614-keV level the new 8^+ yrast state. However, it seems to be difficult to explain why this $10^+\rightarrow8^+\rightarrow6^+\rightarrow4^+$ yrast sequence is so weakly populated. In our analysis of DCO ratios, we confirmed the $\Delta I=2$ character of the 622-keV and 1040-keV γ rays, but for the 500-keV transition we obtained the value $R_{DCO}=0.65(6)$, opposite to $R_{DCO}=1.19(15)$ in Ref. [3], which is closer to the value expected for dipole transitions. The most probable spin assignment would then be 9^- (3654 keV)$\rightarrow7^-$ (2614 keV)$\rightarrow5^-$ (1992 keV) $\rightarrow4^+$ (1492 keV). However, due to the unclear situation, we did not assign spins to these levels.

The revised level scheme of ^{104}Cd obtained in the present work is presented in Fig. 7. For some states, for which no

TABLE I. Lifetimes of excited states in ^{104}Cd. The γ transitions given in the third column were used in the lifetime determination. τ_{DDCM}, τ_{RDDS}, and τ_{DSA} are the values obtained in the DDCM, RDDS, and DSA analysis, respectively, as described in Sec. IV. In the last two columns, the adopted experimental values are compared to the IBBPM results (see text).

E_x (keV)	I^π	E_γ (keV)	τ_{DDCM} (ps)	τ_{RDDS} (ps)	τ_{DSA} (ps)	τ_{SF} (ps)	I_{SF} (%)	τ (ps)	τ_{theo} (ps)
				Positive parity					
658	2^+	658	9(3)					9(3)	7.7
1492	4_1^+	834		<6				<6	1.6
1992	(4_2^+)	500		<10				<10	19.9 [a]
2370	6_1^+	878		<6				<6	1.3
2436	6_2^+	944	84(20)	84(6)				84(6)	7.7
2614		622		39(6)				39(6)	366
2904	8_1^+	533	1170(100)	1280(100)				1230(70) [b]	306
3211	8_2^+	841, 776		<7				<7	6.5
3298	8_3^+	928		1.5(3)				1.5(3)	1.1
3654		1040		<16				<16	0.7
3905	9^+	1001		<150				<150	0.8
4102	10^+	890		3(2)				3(2)	4.9
4737	12_1^+	635		310(30)				310(30)	
4818	12_2^+	717		80(6)				80(6)	
5452	13^+	715		<5				<5	
5793	14^+	341, (974), 1056		3.1(6)				3.1(6)	
6241	15^+	448		1.1(2)				1.1(2)	
7149	16^+	908		<1.7				<1.7	
9202	(18^+)	1036			0.87(14) [c]			0.87(14)	
10439	(20^+)	1236			0.28(1)	0.35(6)	11	0.28(3)	
11866		1426			0.34(2)	0.06(1)	100	<0.42	
				Negative parity					
3726	7_1^-	1356		10(1)				10(1)	
3788	7_2^-	1417		<25				<25	
4040	9_1^-	828		15.0(7)				15.0(7)	
4398	9_2^-	745		$9(\frac{1}{2})$				$9(\frac{1}{2})$	8.5
4743	11_1^-	703	4.8(3)	5.4(2)				5.2(2)	5.5
4812	10^-	772		10(1)				10(1)	7.0
5147	11_2^-	749		<6				<6	3.6
5575	12^-	763	<2	<3				<2	2.7
5674	13^-	931	0.6(3) [c]	<2				0.6(3) [c]	1.0
6331	14^-	756		2.9(2)				2.9(2)	3.7
6664	15^-	990	0.4(1)	<2	0.81(9) [d]			0.81(9)	0.98
7280	16^-	949		1.5(2)				1.5(2)	
7783	17^-	1119		<1	0.54(2)	0.73(4)	60	0.54(5)	
8439	18^-	1159		<1	0.40(2)	0.61(6)	43	0.40(6)	
9090	19^-	1306			0.36(3)	0.35(3)	100	<0.75	
9689	20^-	1251			0.36(3)	0.36(3)	100	<0.76	

[a] Assuming this state to have $I^\pi = 4^+$.
[b] Literature value [6]: $\tau(8_1^+) = 1.15(^{29}_{14})$ ns.
[c] See discussion in Sec. IV C.
[d] From NGTB analysis.

spin information could be deduced from our data, the assignments of de Angelis *et al.* [3] were included.

IV. DETERMINATION OF LIFETIMES

In this section, the determination of nuclear lifetimes from both the plunger and the DSA experiment will be described. In the analysis of the plunger data, two different methods can be employed, which are in a certain sense complementary. In what we call the conventional RDDS analysis, information about the lifetime of a state is deduced from the shape of the decay curve $R(x)$ of a γ transition depopulating this state determined in coincidence with the unshifted part of a tran-

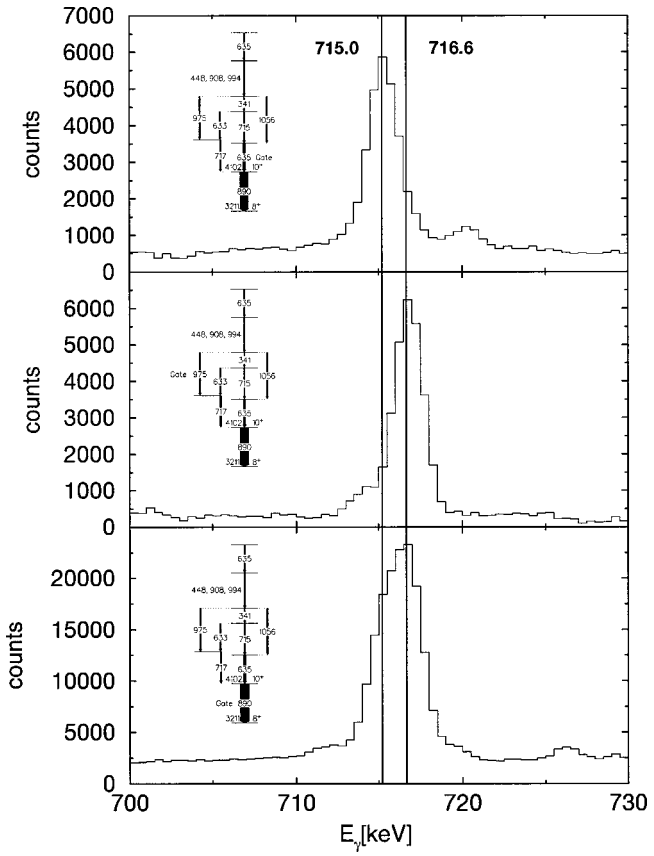

FIG. 4. Line shape of the 717-keV line observed under different gating conditions: (a) gate on 635 keV, (b) gate on 975 keV, (c) gate on 890 keV.

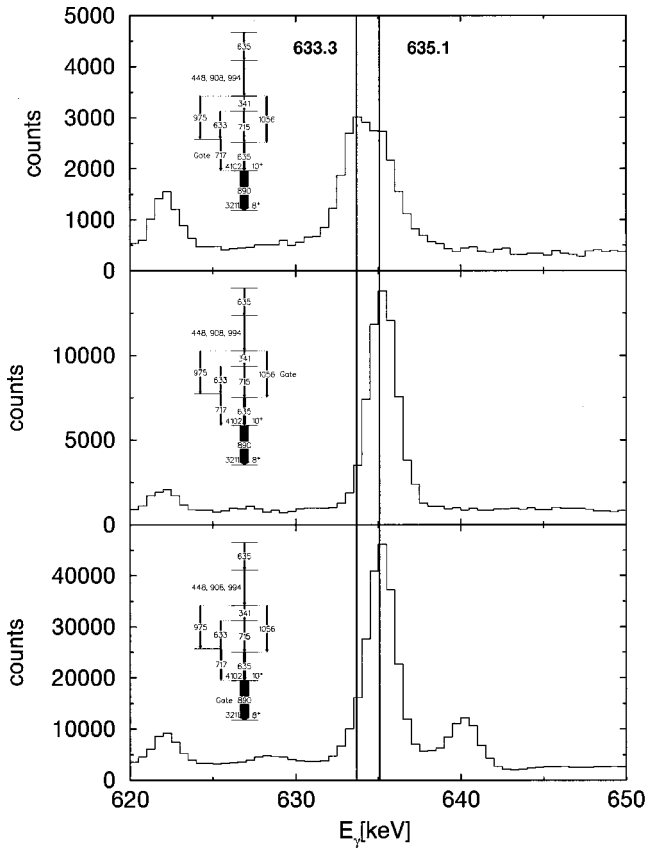

FIG. 5. Line shape of the 635-keV line observed under different gating conditions: (a) gate on 717 keV, (b) gate on 1056 keV, (c) gate on 890 keV.

sition further down (later in time) in the decay sequence, e.g., the ground state transition. Besides the lifetime of the state of interest, this decay curve reflects the complete time history of the feeding of this level, including both known discrete and unknown continuum feeders. To determine the lifetime, the complete feeding pattern including intensities and lifetimes has to be carefully taken into account in the analysis which is always at risk by systematical uncertainties. Despite this drawback, this way of analyzing the data is still very useful since it can be applied even to very weak transitions. Since the gating γ ray can be chosen among all the strong transitions between low-lying states, it is nearly always possible to find a spectrum without contaminations and with enough statistics.

A more elegant way to analyze plunger data is the DDCM introduced some years ago by Böhm *et al.* [11], which will be described in Sec. IV A. In this method, any uncertainties due to an incomplete knowledge of the feeding pattern are excluded. However, as discussed below, it cannot be applied in all cases of interest.

A. DDCM analysis

The lifetime of a state can be deduced for each target-to-stopper distance x independently from the coincidence intensities of γ rays feeding and depopulating the level of interest, thus avoiding systematical uncertainties concerning cascade and side feedings. If γ_{in} denotes a direct feeding transition and γ_{out} a γ ray depopulating the state, the lifetime can be calculated from the equation

$$\tau(x) = \frac{1}{v} \frac{I(\gamma_{out}^{unshifted}, \gamma_{in}^{shifted}; x)}{dI(\gamma_{out}^{shifted}, \gamma_{in}^{shifted}; x)/dx}, \tag{2}$$

where $I(\gamma_{out}^{unshifted}, \gamma_{in}^{shifted}; x)$ is the intensity of the unshifted (stop) component of transition γ_{out} in the coincidence spectrum with the gate set on the Doppler-shifted (flight) component of transition γ_{in}. The lifetime of the state is obtained by averaging the τ values obtained for the distances within the region of highest sensitivity, e.g., the region with large values of both the numerator and the denominator in Eq. (2).

The DDCM method is a very elegant and straightforward way of deducing lifetimes from coincidence data. However, there are two severe limitations. First, the γ transitions involved have to be intense enough to provide a reasonable counting rate in the coincidence spectrum with the gate set on the Doppler-shifted part of the feeding transition. In practice, this means a restriction to the main decay sequence of the level scheme. In addition, it is very important to carefully check these spectra for contaminations that unfortunately occur frequently due to the large energy widths of the gates and the high line density observed in the reaction employed. In

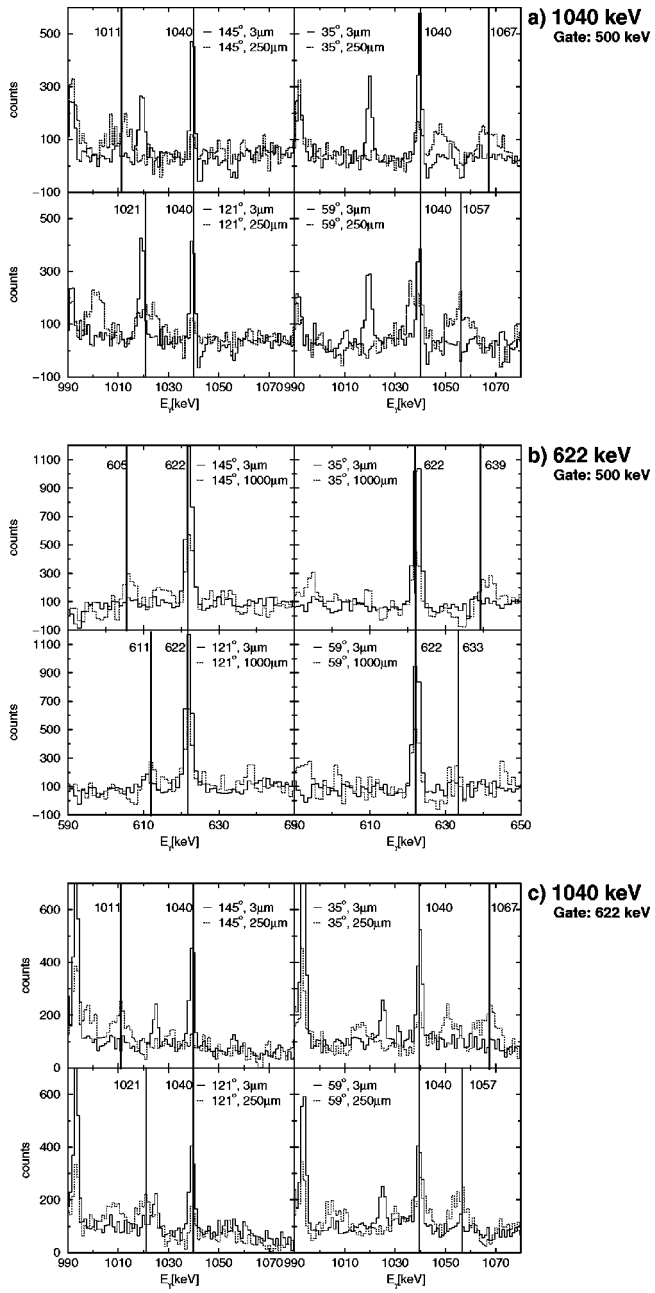

FIG. 6. Partial coincidence spectra taken at four different angles and two different distances showing (a) shifted and unshifted components of the 1040-keV transition in the gate on the 500-keV line, (b) shifted and unshifted components of the 622-keV transition in the gate on the 500-keV line, (c) shifted and unshifted components of the 1040-keV transition in the gate on the 622-keV line.

^{104}Cd, six lifetimes and one additional upper lifetime limit could be deduced using the DDCM technique. The results are listed in Table I and representative for all cases, Fig. 8 illustrates the analysis of the lifetime of the 11^- state at 4743 keV. In Figs. 8(a)–8(c), the intensity of the Doppler-shifted part of the depopulating 703-keV transition, its derivative [the denominator of Eq. (2)] and the intensity of the unshifted component of the same transition are shown, both intensities being determined in the gate on the Doppler-shifted part of the 931-keV feeding transition. The resulting lifetime values as a function of the distance are plotted in Fig. 8(d). For the data shown, the 703-keV γ ray has been detected at $\Theta = 59°$ with respect to the beam. The final lifetimes quoted in Table I were obtained by averaging the values obtained independently from the four data sets corresponding to the four angles of observation $\Theta = 35°$, 59°, 121°, and 145°.

B. RDDS analysis

To obtain lifetime information about additional states, decay curves for most of the γ rays shown in Fig. 7 were determined in coincidence with strong low-lying transitions. From the shape of all these decay curves it became evident that the time structure of this nucleus is dominated by the relatively long lifetimes of the 12_1^+, 12_2^+, 8_1^+, and 6_2^+ levels. As a consequence, many of the curves contain different components and show pronounced steps. To determine lifetimes of individual states from these decay curves, the complete feeding patterns of the states of interest have to be considered. In a first step, the intensities of all γ rays arranged in the level scheme (see Fig. 7) were determined from the efficiency corrected numbers of γ rays detected at 59° with respect to the beam in the sum of the two coincidence spectra with gate on the 834-keV ($4^+ \rightarrow 2^+$) and 658-keV ($2^+ \rightarrow 0^+$) transitions. Then, the effective lifetimes for the 7149-keV (16^+), 7783-keV 17^-, and 8439-keV 18^- states were determined from the fit of a single exponential function to the $R(x)$ curves of the 908-keV, 1119-keV, and 1159-keV transitions, respectively. Starting with this information, for each level of the cascades working from the top to the bottom the relevant feeding pattern with intensities and lifetimes was prepared. Of course, the fit functions become more and more complicated the lower in the level scheme the state of interest is positioned. The difference between the sum of the intensities of all known depopulating transitions and the corresponding sum of all populating γ rays was considered as sidefeeding, with the sidefeeding time treated as a free parameter in the fit. For illustration, the experimental decay curves of the 890-keV, 928-keV, 834-keV, and 828-keV transitions depopulating the 4102-keV 10^+, 3298-keV 8_3^+, 1492-keV 4^+, and 4040-keV 9^- states, respectively, are shown in Fig. 9. The feeding pattern considered in the fit, which is shown as a solid line, is given in the inset of each part of this figure. Figure 9 demonstrates that even the quite complicated shapes of some of the decay curves can be nicely described if the complete feeding is properly taken into account. In the determination of lifetimes, both the individual $R(x)$ curves obtained at the four different angles of observation ($\Theta = 35°$, 59°, 121°, and 145°) as well as the summed $R(x)$ functions (shown in Fig. 9) were fitted. In all cases, the weighted average of the four individual values agreed within the uncertainties with the result from the fit of the summed curve. The results obtained in the analysis of the $R(x)$ curves are summarized in the fifth column of Table I. The quoted uncertainties include the statistical errors and the uncertainties of all parameters in the fit, such as the intensities and times of the discrete feeders and the sidefeeding. For

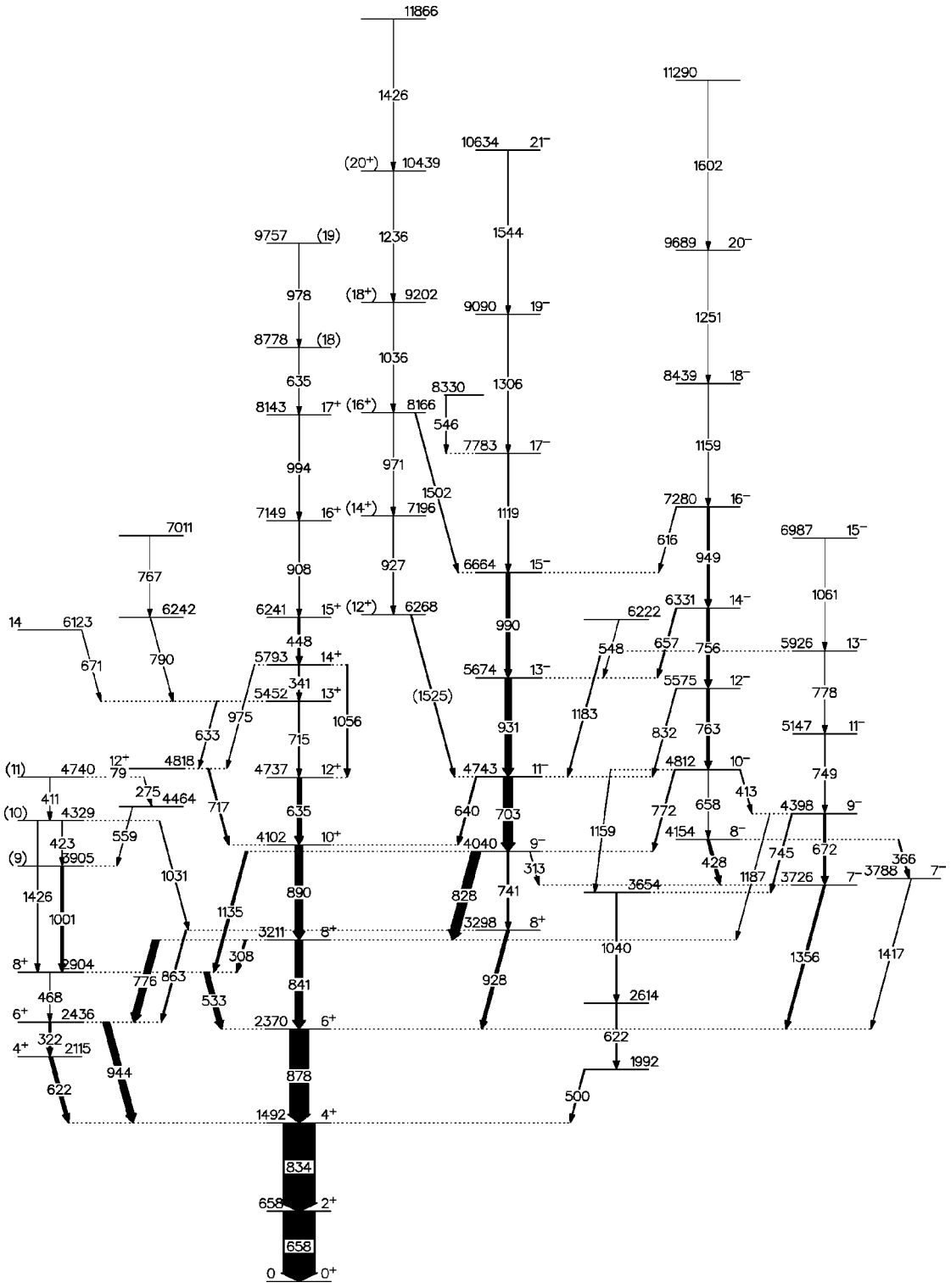

FIG. 7. Revised version of the level scheme of ^{104}Cd obtained in the present work.

many short-lived states, in particular at low spin, only upper limits are given since the decay curves of the depopulating transitions are completely dominated by the feeding from the long-lived states above. Note that in all cases, where both the DDCM and the conventional RDDS analysis could be applied, the agreement between the two results is very good.

C. DSA analysis

In the $E2$ cascades at negative parity, the highest states to be investigated via RDDS are the 17^- and 18^- levels with effective lifetimes shorter than 1 ps. The γ rays depopulating these states are detected mostly Doppler-shifted already at the shortest flight distances of some μm. In order to determine the lifetimes of the highest-spin states, a second experi-

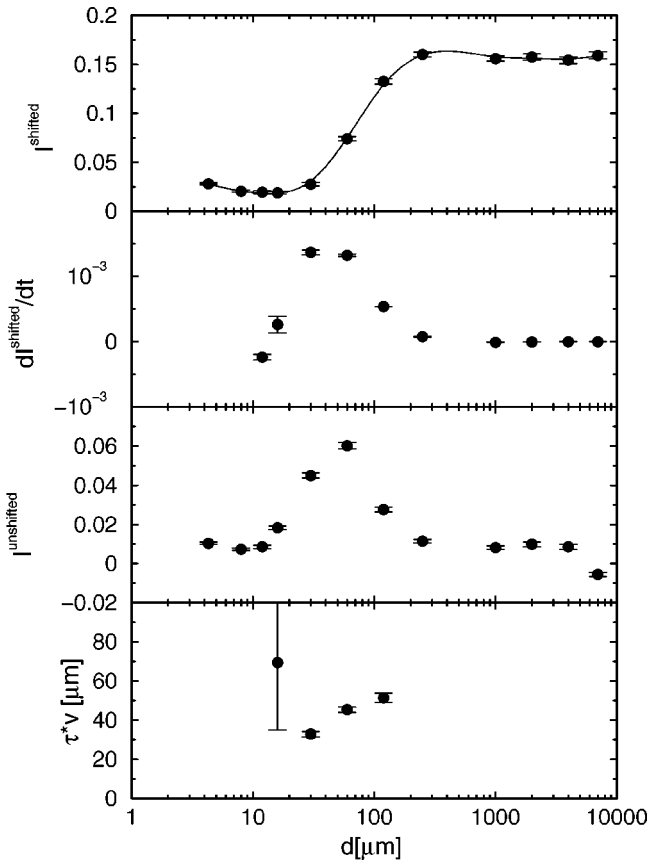

FIG. 8. DDCM analysis of the 11^-, 4743-keV state. (a) Intensity of the Doppler-shifted part of the 703-keV γ ray, (b) its derivative, (c) intensity of the unshifted part of the 703-keV transition, and (d) resulting lifetimes. The intensities of the 703-keV line, observed under $\Theta = 59°$ to the beam, were determined in coincidence with the Doppler-shifted component of the 931-keV feeding transition.

ment with a backed target has been performed (see Sec. II). Indeed, the γ rays with 1119 keV, 1306 keV, 1159 keV, 1251 keV as well as the 1236-keV and 1426-keV transitions at positive parity show Doppler line profiles in the spectra obtained in this experiment. Again, spectra were produced for each of the four angles of observation ($\Theta = 35°$, 59°, 121°, and 145°) separately, with coincidence gates on strong completely unshifted γ rays detected in all detectors of the GASP spectrometer. For fitting the line shapes the program LINESHAPE was used. The program accounts for the energy loss of the beam in the target, the energy and angular distributions of the recoils resulting from kinematics of the particle evaporation process and the stopping power of the recoils in the target and stopper. The stopping power of the beam and the recoils in the target and the backing was treated according to the shell-corrected Northcliffe-Schilling formalism [12], the angular straggling of the recoils was Monte Carlo simulated.

For the highest-lying transitions to be analyzed, namely, the lines at 1426 keV, 1306 keV, and 1251 keV, the line shapes were fitted assuming one feeder with an intensity of 100%. Therefore, the fit function includes three free parameters, the state lifetime, the feeding time, and the area of the line. For the states further down in the cascades, the known feeding pattern was included in the fit in the same way as described in Sec. IV B for the RDDS analysis. As examples, the line shapes of the 1426-keV and 1236-keV transitions observed at 121° to the beam are shown in Figs. 10(a) and 10(b). The line shapes observed at the four different angles of observation were fitted separately and the weighted average of the four values is given in column 6 of Table I. For the final values, the uncertainties of the feeding parameters were taken into account in addition to the statistical errors given in column 6.

In two cases, namely the 18^+ state at 9202 keV and the 15^- level at 6664 keV, the statistics was high enough to allow the application of the narrow gate on transition below (NGTB) method recently proposed by Brandolini and coworkers [13,14]. Like the DDCM method described in Sec. IV A, the NGTB technique avoids all the uncertainties connected to the known and unknown feeding and allows the direct determination of the lifetime of the state under study. The method is based on the comparison of the line shape of the γ transition populating the state of interest under two different coincidence requirements. First, this line shape is observed in coincidence with a completely unshifted transition. Here, any γ ray below the state of interest without Doppler tail can be chosen. Then, the line shape is obtained in coincidence with the unshifted component (stop peak) of the γ ray directly depopulating the level of interest. If this depopulating transition contains both unshifted and shifted components, this coincidence requirement corresponds to a time condition and the observed line shape of the populating γ ray will be modified, namely the Doppler-shifted part will be suppressed. This effect is easily understood since all the coincidences with a shifted depopulating transition and therefore necessarily shifted populating transition are excluded by gating only the unshifted part of the depopulating γ ray. The shorter the lifetime of the intermediate level is, the larger is the suppression effect and the more accurately the lifetime can be deduced. A detailed discussion of this method is given in Refs. [13,14]. Further details specific to our data set including a comparison between results from the NGTB and the DSA analysis in ^{104}In will be presented in a forthcoming publication [15]. To illustrate the method, the suppressed and unsuppressed line profiles of the 1236-keV transition populating the 18^+ state are shown in Figs. 10(c) and 10(d), respectively. The result of the analysis is $\tau(18^+) = 0.87(14)$ ps. The only other case for which a NGTB analysis could be performed is the 15^- state with a lifetime of 0.81(9) ps. This value does not agree with the one obtained in the DDCM analysis, $\tau_{DDCM}(15^-) = 0.4(1)$ ps (compare Sec. IV A). Very recently, Petkov *et al.* [16] pointed out that for very short lifetimes (below 1 ps), the DDCM procedure as described in Sec. IV A leads to lifetimes that are systematically too short. This is due to the fact that when the lifetime becomes comparable to the slowing down time of the recoils in the stopper, the clean separation between a (completely shifted) flight component and a (unshifted) stop component vanishes and a third component, namely, the partly shifted γ rays cannot be neglected any-

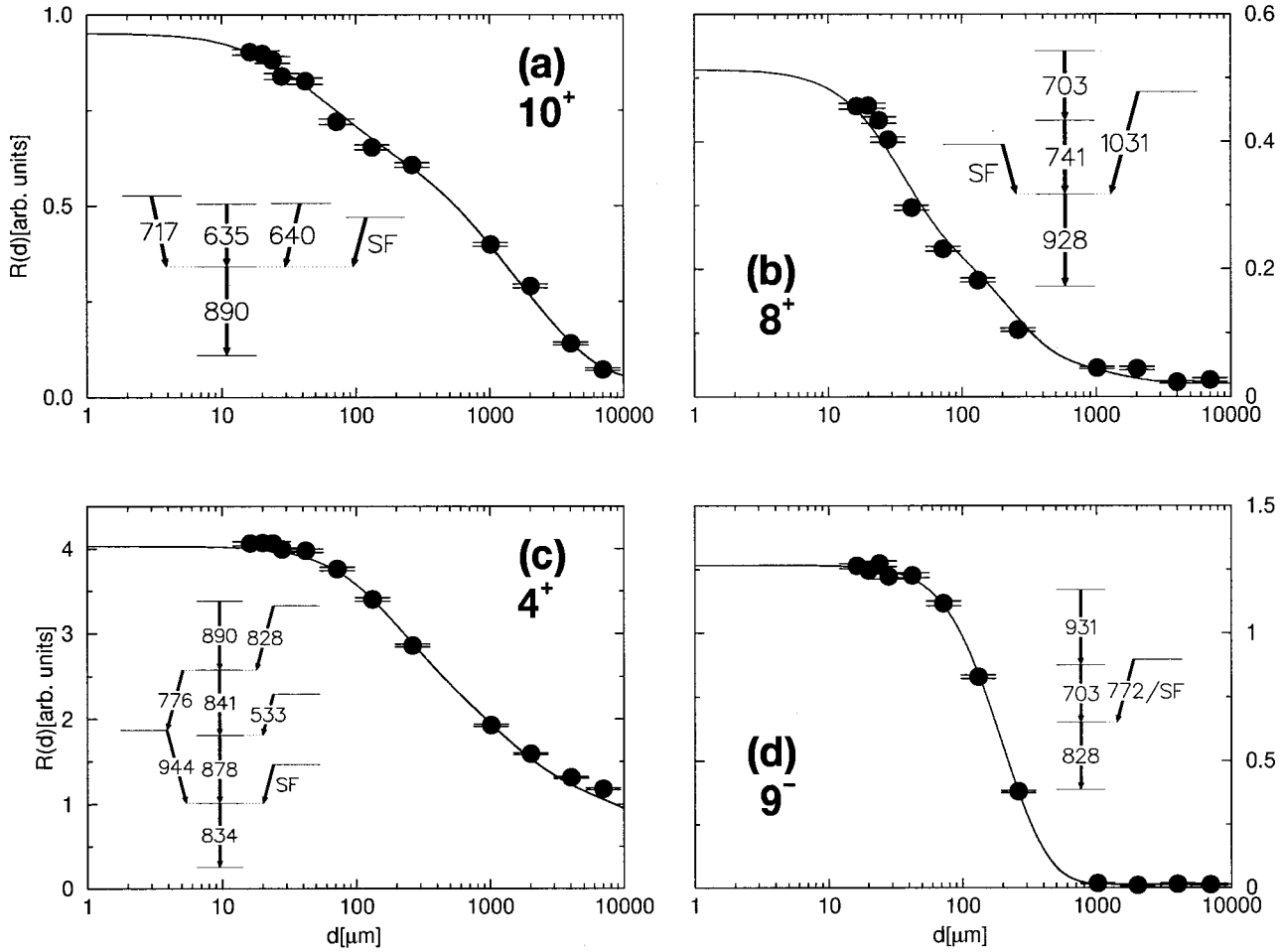

FIG. 9. Decay curves of γ transitions depopulating the 1492-keV 4^+, 3298-keV 8_3^+, 4102-keV 10^+, and 4040-keV 9^- states. The feeding pattern used in the fit (lines) of the experimental data points (filled circles) are shown in the insets.

more. The inclusion of this component in the DDCM analysis [16] leads to an increase of the deduced lifetime and this correction is larger the shorter the lifetime is. Considering these uncertainties, we decided to use the DSA result, $\tau_{DSA}(15^-)=0.81(9)$ ps as the final value. Due to the same effect, the lifetime $\tau_{DDCM}(13^-)=0.6(3)$ ps might be too short, too. However, since the lifetime value is larger in this case, the effect is smaller and covered by the large quoted uncertainty.

To close the experimental section, the experimental transition strengths deduced from the adopted lifetimes quoted in Table I are listed in Table II.

V. CALCULATIONS WITHIN THE INTERACTING BOSON PLUS BROKEN PAIR MODEL

Models that are based on the interacting boson approximation (IBA) [17,18] provide a consistent description of nuclear structure phenomena in spherical, deformed, and transitional nuclei. Many extensions of the original interacting boson model (IBM-1) [18] have been studied. In particular, models have been constructed to describe the physics of high-spin states in nuclei ($10\hbar \leqslant I \leqslant 30\hbar$). In the formulation of these models one has to go beyond the boson approximation and include selected noncollective fermion degrees of freedom. By including part of the original shell-model fermion space through successive breaking of correlated *S* and *D* pairs, the IBM is extended to describe the structure of high-spin states. This extension of the model is especially relevant for transitional regions, where single-particle excitations and vibrational collectivity are dominant modes, and the traditional cranking approach to high-spin physics is not adequate.

The IBBPM, used in the present analysis, has been previously applied in the description of high-spin states in even-even and odd-even nuclei [19–21]. The model is based on the IBM-1 [17]; the boson space consists of *s* and *d* bosons, with no distinction between protons and neutrons. To generate high-spin states, the model allows one or two bosons to be destroyed and to form noncollective fermion pairs, represented by two- and four-quasiparticle states that recouple to the boson core. High-spin states are described in terms of broken pairs.

In a recent paper [3], we have applied the IBBPM in the analysis of two-neutron states in ^{104}Cd. In the present work we extend the model to include, in addition to two broken pairs of identical nucleons, the configurations with two dif-

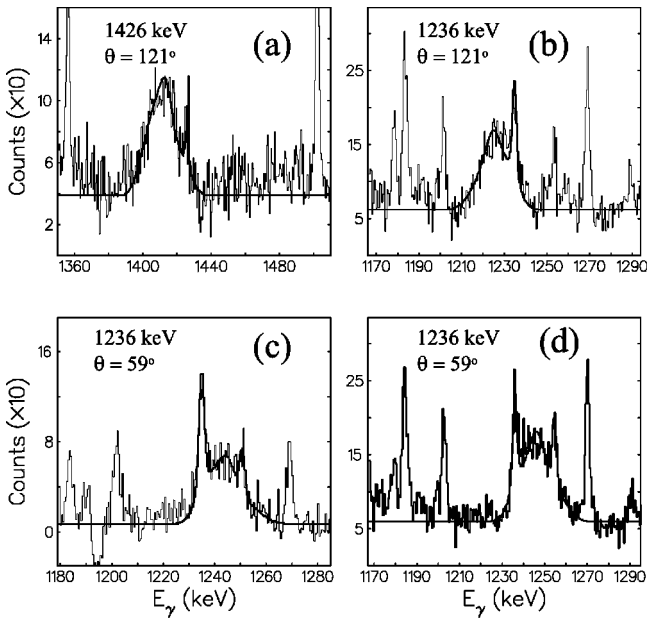

FIG. 10. Doppler line shapes of the (a) 1426-keV transition depopulating the 11866-keV state and (b) 1236-keV γ-ray depopulating the 10 439-keV level observed at 121° to the beam. In (c) and (d), the line profile of the 1236-keV transition observed at 59° to the beam is shown in two different coincidence spectra to illustrate the NGTB analysis of the 18^+ level. The Doppler-shifted component of the line shape observed in coincidence with the unshifted part of the 1036-keV transition (c) is suppressed in comparison to the line shape obtained in coincidence with the completely stopped 927-keV transition (d).

ferent broken pairs, one of protons and one of neutrons. We attempt to simultaneously describe high-spin bands based on two-proton and two-neutron configurations. The advantage of using a model based on the IBA over more traditional approaches based on the cranking approximations, is that no assumption has to be made about the geometrical picture of high-spin bands, and that they result from a consistent calculation of the complete excitation spectrum, which includes also the ground state band.

Most of the parameters of the model Hamiltonian for ^{104}Cd are taken from Ref. [3]. However, new experimental data have enabled an improved parametrization that accounts the mixing of the wave functions of high-spin states. The following parameters have been modified with respect to those used in Ref. [3] (in parentheses we give the values used in Ref. [3]): core parameters $\epsilon=0.887$ MeV (0.658 MeV), $C_0=0.44$ MeV (0 MeV), $C_2=0.233$ MeV (0 MeV), $C_4=0.0333$ MeV (0.117 MeV), neutron quasiparticle energies $E(\nu d_{5/2})=1.211$ MeV (1.113 MeV), $E(\nu g_{7/2})=1.500$ MeV (1.316 MeV), the strength of the neutron pair-breaking interaction $U_2^\nu=0.25$ MeV (0.1 MeV), the strength of the boson-neutron dynamical interaction for positive parity states $\Gamma_0^\nu=0.9$ MeV (0.2 MeV), the strength of the boson-neutron monopole interaction for negative parity states $A_0^\nu=0.03$ MeV (0 MeV). The choice of C_0 and C_2 places the calculated 0_2^+ and 2_2^+ states at excitation energies that are expected from the systematics of Cd isotopes. These parameters have no influence on all other calculated states that are identified among the experimental states. The modifications of the remaining core parameters and of the interaction strengths for positive parity states restore the theoretical spectrum from Ref. [3]. In addition, the resulting wave functions provide a much better description of the mixing between the ground-state band and bands based on the broken pair configurations (for both parametrizations transitions within the bands are almost identical, but the original parameterization sizably underestimates transition intensities between the bands). For example, let us consider the pair breaking interaction V_{mix}, which mixes states with different number of fermions, and conserves only the total number of valence nucleons:

$$
\begin{aligned}
V_{mix}=&-U_0\Bigg\{\sum_{j_1 j_2} u_{j_1}u_{j_2}(u_{j_1}v_{j_2}+u_{j_2}v_{j_1})\\
&\times\langle j_1\|Y_2\|j_2\rangle^2\frac{1}{\sqrt{2j_2+1}}([a_{j_2}^\dagger a_{j_2}^\dagger]^{(0)}s)+\text{H.c.}\Bigg\}\\
&-U_2\Bigg\{\sum_{j_1 j_2}(u_{j_1}v_{j_2}+u_{j_2}v_{j_1})\langle j_1\|Y_2\|j_2\rangle\\
&\times([a_{j_1}^\dagger a_{j_2}^\dagger]^{(2)}\tilde{d})+\text{H.c.}\Bigg\}. \qquad (3)
\end{aligned}
$$

In general, this interaction does not induce sufficient mixing as can be deduced, for example, from observed transition strengths. Equation (3) is the lowest order contribution to a pair-breaking interaction. The first term represents the destruction of one *s* boson and the creation of a fermion pair, while in the second term a *d* boson is destroyed to create a pair of valence fermions. Since the interaction contains only fermion operators of rank 0 and 2, it cannot connect in first order the ground-state band with two-fermion states of higher fermion angular momenta. In order to enhance the mixing, interactions that contain fermion operators of higher rank could be included in the model Hamiltonian. However, such an interaction would also require higher order boson operators, with parameters that cannot be determined from available experimental data, or from the intrinsic structure of the model. Our modifications of the original parametrization [3] (especially Γ_0^ν), partially account for this problem.

The parameters of the boson-proton interactions, the quasiparticle energy and the occupation probability of the $\pi g_{9/2}$ orbital, have been adjusted to reproduce the positive parity states in ^{107}In: $\Gamma_0^\pi=0.9$ MeV, $\Lambda_0^\pi=0$ MeV, $A_0^\pi=-0.1$ MeV, $\chi=-0.9$, $E(\pi g_{9/2})=1.809$ MeV, $v^2(\pi g_{9/2})=0.82$. The strength of the proton pair-breaking interaction is $U_2^\pi=0.2$ MeV.

In Figs. 11 and 12 we display the calculated spectra of positive- and negative-parity states, and compare them with their experimental counterparts. Only the lowest-lying few calculated levels of each angular momentum are included. According to the structure of wave functions, states are classified in bands. We notice here that the 4_2^+ and the 4_3^+ states

TABLE II. Experimental and calculated (IBBPM) transition strengths in ^{104}Cd. To calculate the experimental values from the lifetimes, $\delta=0$ is assumed for all $\Delta I=0,1$ $M1$ transitions.

E_x (keV)	I_i^π	E_γ (keV)	b (%)	I_f^π	σL	$B(\sigma L)$ $(e^2\,\mathrm{fm}^4)/[10^{-3}\mu_N^2]$	$B_{theo}(E2)$ $(e^2\,\mathrm{fm}^4)$	$B_{theo}(M1)$ $[10^{-3}\mu_N^2]$
				Positive parity				
658	2^+	658	100	0^+	$E2$	$735(^{365}_{184})$	859	
1492	4_1^+	834	100	2^+	$E2$	>336	1303	
1992	(4_2^+)	500 [b]	100	4_1^+	$E2$	>2610 [a]	0.8	8.8
				2_1^+	$E2$		6	
2115	4_3^+	622	100	4_1^+	$M1/E2$		0.4	0.3
				4_2^+	$M1/E2$		15	46
				2_1^+	$E2$		0.1	
2370	6_1^+	878	100	4_1^+	$E2$	>246	1172	
2436	6_2^+	322	21(1)	4_3^+	$E2$	$595(^{60}_{50})$	2	
		944	79(1)	4_1^+	$E2$	10.3(8)	142	
2614		622	100		$E2$	$225(^{47}_{37})$	9	
2904	8_1^+	468	5(1)	6_2^+	$E2$	1.4(2)	0.6	
		533	95(1)	6_1^+	$E2$	14.7(8)	62	
3211	8_2^+	308	9.5(6)	8_1^+	$M1$	>25	10	21.4
		776	40(2)	6_2^+	$E2$	>161	310	
		841	50(2)	6_1^+	$E2$	>134	69	
3298	8_3^+	863	29(2)	6_2^+	$E2$	$329(^{85}_{58})$	4	
		928	71(2)	6_1^+	$E2$	$563(^{142}_{95})$	689	
				8_1^+	$M1/E2$		272	306
3654		1040	100		$E2$	>39	879	
3905	9_1^+	1001	100	8_1^+	$M1/E2$		786	20
4102	10^+	890	100	8_2^+	$E2$	$437(^{540}_{180})$	245	
				8_3^+	$E2$		54	
				8_1^+	$E2$		4	
4329	10_2^+	423		9_1^+	$M1/E2$		219	78
		1031		8_3^+	$E2$		45	
		1426		8_1^+	$E2$		484	
4737	12_1^+	635	100	10^+	$E2$	26(4)		
4818	12_2^+	717	100	10^+	$E2$	54(7)		
5452	13^+	633	40(4)	12_2^+	$M1$	>16		
		715	60(4)	12_1^+	$M1$	>17		
5793	14^+	341	25(2)	13^+	$M1$	$114(^{29}_{20})$		
		974	11(4)	12_2^+	$E2$	31(13)		
		1056	65(3)	12_1^+	$E2$	130(26)		
6241	15^+	448	100	14	$M1$	$580(^{130}_{90})$		
7149	16^+	908	100	15	$M1$	>42		
9202	(18^+)	1036	100	16^+	$E2$	786(126)		
10439	(20^+)	1236	100	(18^+)	$E2$	1010(108)		
11866		1426	100	(20^+)	$E2$ [c]	>330 [c]		
				Negative parity				
3726	7_1^-	1356	100	6_1^+	$E1$	$2.52(30)\times10^{-5}$		
3788	7_2^-	1417	100	6_1^+	$E1$	$>8.3\times10^{-6}$		
4040	9_1^-	313	2.5(3)	7_1^-	$E2$	448(52)	2	
		741	11(1)	8_3^+	$E1$	$1.18(9)\times10^{-5}$		
		828	70(1)	8_2^+	$E1$	$5.21(26)\times10^{-5}$		
		1135	17(1)	8_1^+	$E1$	$4.94(38)\times10^{-6}$		
4154	8_1^-			9_1^-	$M1/E2$		2	53
		428		7_1^-	$M1/E2$		0.7	0.02

TABLE II. (*Continued*).

E_x (keV)	I_i^π	E_γ (keV)	b (%)	I_f^π	σL	$B(\sigma L)$ $(e^2\,\mathrm{fm}^4)/[10^{-3}\mu_N^2]$	$B_{theo}(E2)$ $(e^2\,\mathrm{fm}^4)$	$B_{theo}(M1)$ $[10^{-3}\mu_N^2]$
4398	9_2^-	672	76(2)	7_1^-	$E2$	$508(^{58}_{113})$	605	
		745	24(2)		$E2$	$92(^{12}_{22})$		
4743	11_1^-	640	11(1)	10_2^+	$E1$	$5.33(43)\times10^{-5}$		
		703	89(1)	9_1^-	$E2$	825(35)	873	
4812	10_1^-	658		8_1^-	$E2$	660 [d]	859	
		772		9_1^-	$M1/E2$		3	1.2
		413		9_2^-	$M1/E2$		0.1	0.3
5147	11_2^-	749	100	9_2^-	$E2$	>538	966	
5575	12^-	763	84(5)	10^-	$E2$	>1239	1113	
		833	16(5)	11_1^-	$M1$	>3.7	2	1.3
5674	13_1^-	931	100	11_1^-	$E2$	$1893(^{1674}_{641})$	1142	
5926	13_2^-	778		11_2^-	$E2$		763	
		1183		11_1^-	$E2$		0.02	
6331	14^-	658	26(3)	13_1^-	$M1$	17.7(2.5)	2	0.8
		756	74(3)	12^-	$E2$	847(70)	804	
				13_2^-	$M1/E2$		3	11
6664	15^-	990	100	13_1^-	$E2$	1059(118)	844	
				14_1^-	$M1/E2$		2	69
7280	16^-	616	12(1)	15^-	$M1$	$19.7(^{3.6}_{2.8})$		
		949	88(1)	14^-	$E2$	$622(^{96}_{74})$		
7783	17^-	1119	100	15_2^-	$E2$	861(80)		
8439	18^-	1159	100	16^-	$E2$	975(146)		
9090	19^-	1306	100	17^-	$E2$	>286		
9689	20^-	1251	100	18^-	$E2$	>350		

[a]Assuming this state to have $I^\pi=4^+$.

[b]Transition not observed but calculated to have a branching $b>5\%$.

[c]Assuming the 11866 keV state to have spin 22^+.

[d]Since 658 keV is doublet with the $2^+\rightarrow0^+$ transition, the branching ratio cannot be determined and we quote the maximal $B(E2)$ assuming $b=100\%$.

cannot be assigned to any band. Their wave functions are strong mixtures of the $(\nu d_{5/2}\ \nu g_{7/2})$ and the $(\nu d_{5/2})^2$ configurations.

The electromagnetic properties (Tables I and II) have been calculated with the effective charges and gyromagnetic factors that were used in Ref. [22] for ^{106}Ag: $e^\pi=1.5$, $e^\nu=0.5$, $e^{vib}=2.1$, $\chi=-0.9$, $g_l^\pi=1.0$, $g_l^\nu=0$, $g_s^\pi=0.4$ $g_s^{\pi,free}=2.234$, $g_s^\nu=0.4$ $g_s^{\nu,free}=-1.530$. $g_R=Z/A=0.462$. Only e^{vib} was slightly modified in order to reproduce the experimental value of $Q(2_1^+)$ in ^{106}Cd. The boson charge e^{vib} is defined according to Ref. [23].

The excitation energies of the collective vibrational states 2_1^+ at 0.658 MeV, 4_1^+ at 1.492 MeV, and 6_1^+ at 2.370 MeV, are reproduced by the present calculation (in the following discussion, as well as in Tables I and II, the states are labeled in accordance with the experimental ordering). Above the 6_1^+ state configurations based on neutron or proton broken pairs dominate the states along the yrast line. The experimental levels 6_2^+ at 2.436 MeV, 8_2^+ at 3.211 MeV, and 10_1^+ at 4.102 MeV excitation energy are predominantly based on the $(\nu d_{5/2}\ \nu g_{7/2})$ configuration. The wave function of the theoretical state that corresponds to the level 8_2^+ has only 17% contribution from the purely collective configurations characteristic for the ground-state band. On the other hand, the theoretical state identified with the 8_3^+ level contains 61% collective ground-state band components, and the remaining amplitude is a mixture of $(\pi g_{9/2})^2$ and $(\nu d_{5/2}\ \nu g_{7/2})$ components. We have therefore assigned the experimental 8_3^+ state to the ground-state band. This assignment is also based on the decay pattern of the levels at 3.211, 3.298, and 4.102 MeV. The transitions are better described when the levels at 3.211 and 4.102 MeV are not assigned to the ground-state band structure. However, due to our simplified choice of the mixing interaction, some discrepancies are still present. The calculation overestimates the contribution of the $(\pi g_{9/2})^2$ configurations in the wave function of the 8_3^+ state, while it underestimates the contribution of $(\nu d_{5/2}\ \nu g_{7/2})$. This results in the strong transition $8_3^+\rightarrow8_1^+$, while the calculated transition $8_3^+\rightarrow6_2^+$ is too weak. The 4^+ level at 2.115-MeV excitation energy has a complex structure based on the $(\nu d_{5/2}\ \nu g_{7/2})$ and $(\nu d_{5/2})^2$ configurations. The transitions to and from this state are characterized by small transition prob-

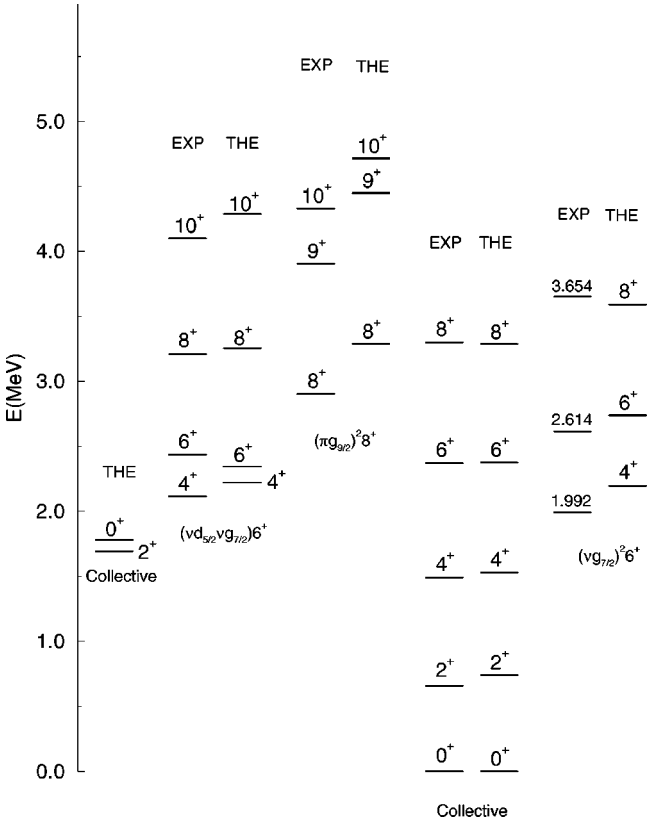

FIG. 11. Positive-parity states in ^{104}Cd compared with the results of the IBBPM calculation. We notice that the 4_2^+ and the 4_3^+ states cannot be assigned to any band. Their wave functions are strong mixtures of the $(\nu d_{5/2}\ \nu g_{7/2})$ and the $(\nu d_{5/2})^2$ configurations.

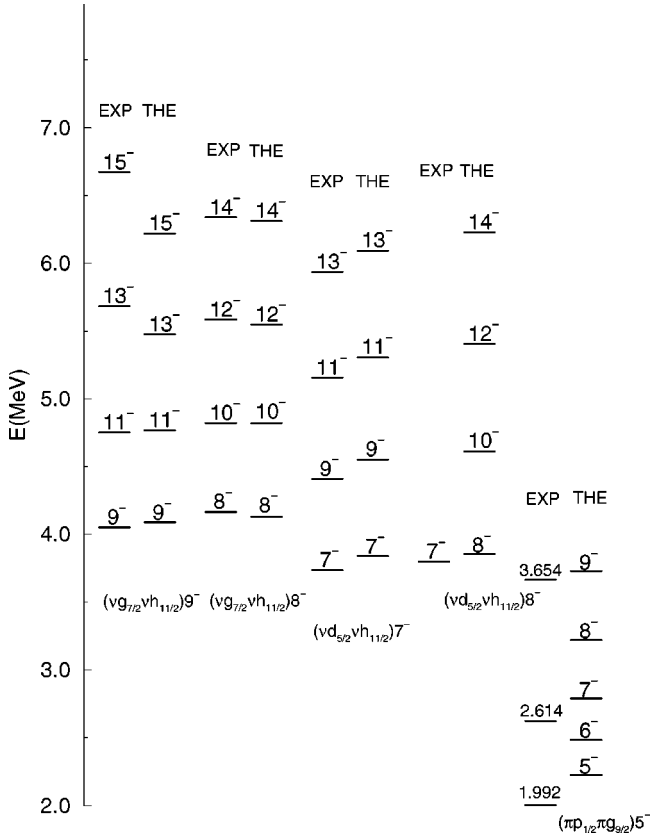

FIG. 12. Negative-parity states in ^{104}Cd compared with the results of the IBBPM calculation.

abilities that are sensitive to the details of the model parametrization and to contributions from outside the model space.

To the three levels 8_1^+ at 2.904 MeV, 9_1^+ at 3.905 MeV, and 10_2^+ at 4.329 MeV, we assign the $(\pi g_{9/2})^2$ structure. The assignment is supported by the systematics of excitation energies in neighboring odd-A In isotopes. The decay pattern of the bandhead ($8_1^+ \rightarrow 6_2^+$ and $8_1^+ \rightarrow 6_1^+$) is well reproduced by the IBBPM calculation. Both transitions proceed mainly through collective ground-state band components. The absolute values of the transition probabilities depend on the amount of ground-state band components in the wave function of the 8_1^+ state. The percentage of collective components in the 6_2^+ state, which is predominantly $(\nu d_{5/2}\ \nu g_{7/2})$, determines the relative intensities of the two transitions from 8_1^+.

Above approximately 4-MeV excitation energy, the spectra of positive-parity states will be affected by configurations that are not included in the model space of the present calculation. In this region, therefore, we cannot compare the experimental spectra with results of model calculations.

The sequence of experimental levels at 1.992-, 2.614-, and 3.654-MeV excitation energy (notice that these levels have been placed in a different way in Ref. [3]), poses a problem for a theoretical interpretation. For positive parity the lowest state must have $I \leqslant 6$. The 5^+ and yrast 6^+ state contradict the systematics of Cd isotopes and the predictions of the IBBPM calculation. The only possibility, therefore, for the lowest level is a 4^+ state. We tentatively assign 4_2^+ with the mixed $(\nu d_{5/2}\ \nu g_{7/2})$ and $(\nu d_{5/2})^2$ structure to the 1.992-MeV level, and 6_3^+ and 8_4^+ with the $(\nu g_{7/2})^2$ structure for the 2.614- and 3.654-MeV levels. This assignment results in a rather long lifetime for the 6_3^+ state (probably due to problems with mixing in the wave functions, as already discussed). This also means that the transition from the 10^- state at 4.812 MeV, to the highest-lying level in this sequence, has to be an $M2$. But most problematic, an 8^+ assignment to the 3.654-MeV level is in contradiction to the $\Delta I = 2$ character of the 745-keV transition depopulating the 9^- state at 4.398 MeV. However, the assignment of negative parity to the 1.992-, 2.614-, and 3.654-MeV levels poses even more problems. Firstly, this requires a $\pi p_{1/2}$ quasiparticle energy ≈ 0.5 MeV lower than expected from the systematics of odd-A In isotopes and in addition very strong boson-proton interactions. Secondly, a state 5^- was not observed at such a low excitation energy in the whole sequence of Cd isotopes (in heavier isotopes it was observed at ≈ 2.6-MeV excitation energy). Including in our model space the $\pi p_{1/2}$ orbital with the quasiparticle energy $E(\pi p_{1/2}) = 2.0$ MeV, occupation probability $v^2(\pi p_{1/2}) = 0.90$ and adjusting the strengths of boson-proton interactions for negative-parity states $\Gamma_0^\pi = 1.3$ MeV and $A_0^\pi = 0.15$ MeV, we can tentatively assign the 5^-, 7^-, and 9^- states based on the $(\pi p_{1/2}\ \pi g_{9/2})$ configuration to the experimental levels at 1.992, 2.614, and 3.654 MeV, respectively (Fig. 12).

The calculated lifetimes 16.5 ps for the 7^- and 2.4 ps for the 9^- level are in agreement with our data but the decay pattern is different from the observed one. We predict that the $E2$ and $M1$ transition intensities within this band are of the same order of magnitude, i.e., that 6^- and 8^- levels should be populated. As discussed in Sec. III, we obtained $R_{DCO}=0.65(6)$ for the 500-keV γ ray implying $\Delta I=1$ for the 1992-keV→1492-keV transition. This additionally makes questionable the negative-parity assignment for these levels.

To the sequence of negative-parity states 9_1^-, 11_1^-, 13_1^-, 15_1^-, at excitation energies 4.040, 4.743, 5.674, and 6.664 MeV, respectively, we assigned the $(\nu g_{7/2}\ \nu h_{11/2})9^-$ structure. Due to the truncation of the model basis, we are not able to calculate states with higher angular momenta, but it is obvious that also the levels at 7.783, 9.090, and 10.634 MeV belong to this $\Delta I=2$ band. The calculated electromagnetic properties of the $(\nu g_{7/2}\ \nu h_{11/2})9^-$ band are in perfect agreement with experimental data. In the present version of the model we are not able to calculate $E1$ transitions, and therefore the theoretical lifetime of the bandhead 9_1^- could not be determined. From the analysis of excitation energies, transition intensities, and lifetimes, the levels 8_1^-, 10_1^-, 12_1^-, 14_1^-, at excitation energies 4.154, 4.812, 5.575, and 6.331 MeV, respectively, are identified as the $(\nu g_{7/2}\ \nu h_{11/2})8^-$ structure. Again, due to the limited model space, we are not able to calculate higher-lying members of this band, but it is probable that levels at excitation energies 7.280, 8.439, 9.689, and 11.290 MeV have the same structure. The sequence of transition energies does not seem to indicate a breaking of another pair.

We assign the $(\nu d_{5/2}\ \nu h_{11/2})7^-$ structure to the sequence of levels 7_1^-, 9_2^-, 11_2^-, and 13_2^-, at excitation energies 3.726, 4.398, 5.147, and 5.926 MeV, respectively. In addition, we predict another band of similar structure, based on the $(\nu d_{5/2}\ \nu h_{11/2})8^-$ configuration. This band was not seen in the experiment, and according to our calculations it cannot be strongly populated from the observed levels. The calculated 8^- bandhead is found very close in excitation energy to the observed 7^- level at 3.788 MeV, which has no theoretical counterpart. This level is very probably based on a two-neutron configuration. Its decay pattern and lifetime are not compatible with a two-proton structure. In this region of excitation energy our calculation does not predict additional 7^- states, it could well be that the state at 3.788-MeV level is in fact an 8^-. This assignment, however, contradicts the $E1$ character of the 1.417-MeV transition to the 6_1^+ state, though an $M2$ transition would probably result in a similar lifetime.

We notice that the calculated transition $8_1^-\rightarrow 7_1^-$ is very weak, and consequently the lifetime of the 8_1^- state is very long. This is caused by the choice of the $M1$ operator, which was used in its simple standard form. It is well known [24] that the tensor term $(Y_2\sigma)_1$ in the $M1$ operator enhances the l-forbidden $M1$-transition intensity by several orders of magnitude. Since the $8_1^-\rightarrow 7_1^-$ transition is $\nu g_{7/2}\rightarrow \nu d_{5/2}$ l forbidden, it will be very sensitive to the form of the $M1$ operator.

VI. CONCLUSIONS

A large number of electromagnetic transition rates in the vibrational nucleus ^{104}Cd have been measured using the recoil-distance Doppler-shift and Doppler-shift attenuation methods. With only a few exceptions, the agreement between the experimental results and calculations in the framework of the interacting boson plus broken pair model is rather satisfactory. Two-neutron configurations based on the $d_{5/2}$, $g_{7/2}$, and $h_{11/2}$ orbitals could be assigned to the observed structures at negative parity and at positive parity, both two-proton $(\pi g_{9/2})^2$ and two-neutron $(\nu d_{5/2}\ \nu g_{7/2})$ configurations were identified besides the collective vibrational sequence. The recoil-distance data required a revision of the published level scheme of ^{104}Cd [3] in two regions and also proved that the magnetic dipole band proposed in [5] does not exist. The structure of the 1992-, 2614-, and 3654-keV states, for which no unambiguous spin assignments were possible, remains a puzzle.

ACKNOWLEDGMENTS

We are most grateful to the crew of the tandem accelerator at the LNL Legnaro for their friendly and efficient cooperation. This work was supported by Deutsches Bundesministerium für Bildung, Wissenschaft, Forschung und Technologie (BMBF).

[1] R. Rodriguez-Guzman, J. L. Egido, and L. M. Robledo, Phys. Rev. C **62**, 054319 (2000).

[2] R. Rodriguez-Guzman (private communication).

[3] G. de Angelis, C. Fahlander, D. Vretenar, S. Brant, A. Gadea, A. Algora, Y. Li, Q. Pan, E. Farnea, D. Bazzacco, G. Bonsignori, F. Brandolini, M. de Poli, D. De Acuna, S. Lunardi, G. Maron, D. R. Napoli, P. Pavan, C. M. Petrache, C. Rossi Alvarez, P. Spolaore, and G. Vedovato, Phys. Rev. C **60**, 014313 (1999).

[4] W. Klamra, E. Adamides, R. A. Bark, B. Cederwall, C. Fahlander, B. Fogelberg, A. Gizon, J. Gizon, H. Grawe, E. Ideguchi, D. Jerrestam, A. Johnson, R. Julin, S. Juutinen, W. Kaczmarczyk, A. Kerek, J. Kownacki, S. Mitarai, L. O. Morlin, J. Nyberg, M. Piiparinen, R. Schubart, D. Seweryniak, G. Sletten, S. Törmänen, A. Virtanen, and R. Wyss, Z. Phys. A **352**, 117 (1995).

[5] D. G. Jenkins, R. Wadsworth, J. A. Cameron, M. P. Carpenter, C. J. Chiara, R. M. Clark, M. Devlin, P. Fallon, D. B. Fossan, I. M. Hibbert, R. V. F. Janssens, V. P. Janzen, R. Krücken, D. R. La Fosse, G. J. Lane, T. Lauritsen, I. Y. Lee, A. O. Macchiavelli, C. M. Parry, D. G. Sarantites, J. M. Sears, D. Seweryniak, J. F. Smith, K. Starosta, D. Ward, I. Wiedenhoever, A. N. Wilson, J. N. Wilson, and S. Frauendorf, nucl-ex/0007004.

[6] W. Andrejtscheff, L. K. Kostov, H. Rotter, H. Prade, F. Stary, M. Senba, N. Tsoupas, Z. Z. Ding, and P. Raghavan, Nucl. Phys. **A437**, 167 (1985).

[7] D. Bazzacco, Report No. AECL 10613, 1992 (unpublished).

[8] A. Dewald, P. Sala, R. Wrzal, G. Böhm, D. Lieberz, G. Siems, R. Wirowski, K. O. Zell, A. Gelberg, P. von Brentano, P. Nolan, A. J. Kirwan, J. Bishop, R. Julin, A. Lampinen, and H. Hattula, Nucl. Phys. **A545**, 822 (1992).
[9] D. Kast, A. Jungclaus, K. P. Lieb, M. Górska, G. de Angelis, P. G. Bizzeti, A. Dewald, C. Fahlander, H. Grawe, R. Peusquens, M. De Poli, and H. Tiesler, Eur. Phys. J. A **3**, 115 (1998).
[10] R. Schubart, H. Grawe, J. Heese, H. Kluge, K. H. Maier, and M. Schramm, Z. Phys. A **352**, 373 (1995).
[11] G. Böhm, A. Dewald, P. Petkov, and P. von Brentano, Nucl. Instrum. Methods Phys. Res. A **329**, 248 (1993); A. Dewald, S. Harissopulos, and P. von Brentano, Z. Phys. A **334**, 163 (1989).
[12] L. C. Northcliffe and R. F. Schilling, Nucl. Data, Sect. A **7**, 233 (1970).
[13] F. Brandolini and R. V. Ribas, Nucl. Instrum. Methods Phys. Res. A **417**, 150 (1998).
[14] F. Brandolini, S. M. Lenzi, D. R. Napoli, R. V. Ribas, H. Somacal, C. A. Ur, D. Bazzacco, J. A. Cameron, G. de Angelis, M. de Poli, C. Fahlander, A. Gadea, S. Lunardi, G. Martinez-Pinedo, N. H. Medina, C. Rossi Alvarez, J. Sanchez Solano, and C. E. Svensson, Nucl. Phys. **A642**, 387 (1998).
[15] O. Yordanov *et al.*, Eur. Phys. J. A (submitted).
[16] P. Petkov, D. Tonev, J. Gableske, A. Dewald, T. Klemme, and P. von Brentano, Nucl. Instrum. Methods Phys. Res. A **431**, 208 (1999).
[17] F. Iachello and A. Arima, *The Interacting Boson Model* (Cambridge University Press, Cambridge, 1987).
[18] A. Arima and F. Iachello, Phys. Rev. Lett. **35**, 1069 (1975).
[19] F. Iachello and D. Vretenar, Phys. Rev. C **43**, R945 (1991).
[20] D. Vretenar, G. Bonsignori, and M. Savoia, Phys. Rev. C **47**, 2019 (1993).
[21] D. Vretenar, G. Bonsignori, and M. Savoia, Z. Phys. A **351**, 289 (1995).
[22] W. Andrejtscheff, L. K. Kostov, P. Petkov, S. Brant, V. Paar, V. Lopac, G. Boehm, J. Eberth, R. Wirowski, and K. O. Zell, Nucl. Phys. **A516**, 157 (1990).
[23] Y. Tokunaga, H. Seyfarth, O. W. B. Schult, S. Brant, V. Paar, D. Vretenar, H. G. Börner, G. Barreau, H. Faust, Ch. Hofmeyr, K. Schreckenbach, and R. A. Meyer, Nucl. Phys. **A430**, 269 (1984).
[24] V. Paar and S. Brant, Phys. Lett. **74B**, 297 (1978).